

1 Climatology, seasonality and trends of oceanic coherent 2 eddies

3 **Josué Martínez-Moreno¹, Andrew McC. Hogg¹, and Matthew England²**

4 ¹Research School of Earth Science and ARC Center of Excellence for Climate Extremes, Australian
5 National University, Canberra, Australia

6 ²Climate Change Research Centre (CCRC), UNSW Australia, Sydney NSW, Australia

7 **Key Points:**

- 8 • Kinetic energy of coherent eddies contain around 50% of the surface ocean kinetic
9 energy budget.
- 10 • Seasonal cycle of the number of coherent eddies and coherent eddy amplitude re-
11 veal a 3-6 month lag to wind forcing
- 12 • Seasonal lag between the number of coherent eddies and eddy amplitude.
- 13 • The coherent eddy amplitude has increase at a rate of 3 cm per decade since 1993.

14 **Abstract**

15 Ocean eddies influence regional and global climate through mixing and transport
 16 of heat and properties. One of the most recognizable and ubiquitous feature of oceanic
 17 eddies are vortices with spatial scales of tens to hundreds of kilometers, frequently re-
 18 ferred as “mesoscale eddies” or “coherent eddies”. Coherent eddies are known to trans-
 19 port properties across the ocean and to locally affect near-surface wind, cloud proper-
 20 ties and rainfall patterns. Although coherent eddies are ubiquitous, yet their climatol-
 21 ogy, seasonality and long-term temporal evolution remains poorly understood. Thus, we
 22 examine the kinetic energy contained by coherent eddies and we present the annual, in-
 23 terannual, and long-term changes of automatically identified coherent eddies from satel-
 24 lite observations from 1993 to 2018. Around 50% of the kinetic energy contained by ocean
 25 eddies corresponds to coherent eddies. Additionally, a strong hemispherical seasonal cy-
 26 cle is observed, with a 3–6 months lag between the wind forcing and the response of the
 27 coherent eddy field. Furthermore, the seasonality of the number of coherent eddies and
 28 their amplitude reveals that the number of coherent eddies responds faster to the forc-
 29 ing (~3 months), then the coherent eddy amplitude (which is lagged by ~6 months). Our
 30 analysis highlights the relative importance of the coherent eddy field in the ocean ki-
 31 netic energy budget, implies a strong response of the eddy number and eddy amplitude
 32 to forcing at different time-scales, and showcases the seasonality, and multidecadal trends
 33 of coherent eddy properties.

34 **Plain language summary**

35 **1 Introduction**

36 Mesoscale ocean variability with spatial scales of tens to hundreds of kilometers is
 37 comprised of processes such as vortices, waves, and jets (Ferrari & Wunsch, 2009; Fu et
 38 al., 2010). These mesoscale processes are highly energetic, and they play a crucial role
 39 in the transport of heat, salt, momentum, and other tracers through the ocean (Wun-
 40 sch & Ferrari, 2004; Wyrtki et al., 1976; Gill et al., 1974). Possibly, the most recogniz-
 41 able and abundant process observed from satellites is mesoscale vortices. Although mesoscale
 42 vortices are commonly referred to in literature as “mesoscale eddies”, this term is also
 43 often used to describe the total mesoscale ocean variability (the time-varying component
 44 of the mesoscale flow), thus, here we will refer to mesoscale vortices as *coherent eddies*.

45 Coherent eddies are quasi-circular currents. According to their rotational direction,
46 the sea surface height anomaly within a coherent eddy can have a negative or positive
47 sea surface height anomaly (cold-core and warm-core coherent eddies, respectively). This
48 characteristic sea surface height signature of coherent eddies has been utilized to auto-
49 matically identify and track coherent eddies from satellite altimetry (Cui et al., 2020;
50 Martínez-Moreno et al., 2019; Ashkezari et al., 2016; Faghmous et al., 2015; Chelton et
51 al., 2007). Automated identification algorithms of coherent eddies have shown their ubiq-
52 uituity in the oceans, with a predominant influence at hotspots of eddy activity such as bound-
53 ary currents and the Antarctic Circumpolar Current. In these regions, Chelton et al. (2011)
54 estimated that coherent eddies contribute around 40–50% of the mesoscale kinetic en-
55 ergy (Chelton et al., 2011) and thus a significant fraction of the total kinetic energy (Fer-
56 rari & Wunsch, 2009). Although this unique estimate showcases the importance of the
57 mesoscale coherent eddy field, the energy contained by coherent eddies was estimated
58 by extracting the geostrophic velocities within the detected coherent eddies, thus it is
59 possible it may contain energy from other processes. Coherent eddies are not only abun-
60 dant and may have a large proportion of the surface kinetic energy budget, but they are
61 also essential to ocean dynamics as concluded by many previous studies (Patel et al., 2020;
62 Schubert et al., 2019; Pilo et al., 2015; Frenger et al., 2015, 2013; Beron-Vera et al., 2013;
63 Siegel et al., 2011; Hogg & Blundell, 2006).

64 There is broad consensus that mesoscale eddy kinetic energy has a pronounced sea-
65 sonal variability (Uchida et al., 2017; Kang & Curchitser, 2017; Qiu & Chen, 2004; Qiu,
66 1999). Several hypotheses have been proposed to explain this seasonality including: sea-
67 sonal variations of atmospheric forcing (Sasaki et al., 2014), seasonality of the mixed layer
68 depth (Qiu et al., 2014; Callies et al., 2015), seasonality of the intensity of barotropic in-
69 stability (Qiu & Chen, 2004), the variability of the baroclinic instability due to the sea-
70 sonality of the vertical shear (Qiu, 1999), and a seasonal lag of the inverse energy cas-
71 cade (energy is transported between scales from small to large; Arbic et al., 2013) in com-
72 bination with the presence of a front in the mixed layer, which can lead to a seasonal
73 cycle of the baroclinic instability (Qiu et al., 2014). On one hand, processes such as barotropic
74 and baroclinic instabilities control the seasonality of coherent eddies in the ocean. On
75 the other hand, recent studies using observations and eddy-permitting climate models
76 suggest several long-term adjustments of the global ocean capable of long-term changes
77 in the coherent eddy field. Such readjustments include a multidecadal increase in the ocean

78 stratification resulted from temperature and salinity changes (Li et al., 2020), a horizontal
79 readjustment of the sea surface temperature gradients (Ruela et al., 2020; Bouali et
80 al., 2017; Cane et al., 1997), and an intensification of the kinetic energy, eddy kinetic en-
81 ergy, and mesoscale eddy kinetic energy over the last 3 decades as a consequence of an
82 increase in wind forcing (Hu et al., 2020; Wunsch, 2020; Martínez-Moreno et al., 2021).
83 All these seasonal factors and long-term readjustments directly influence the annual and
84 decadal response of the coherent eddy field, however, the seasonality of the coherent com-
85 ponent of the eddy kinetic energy, as well as the seasonal cycle and trends of the coher-
86 ent eddy statistics remain unknown.

87 Here we present a new global climatology of the coherent eddy kinetic energy by
88 reconstructing the coherent eddy signature from satellite observations. Our climatology
89 documents the seasonal cycle of the coherent eddy kinetic energy, and seasonal cycle and
90 long-term trends of the coherent eddy properties over the satellite record. Moreover, we
91 conduct more detail analysis in regions where coherent eddies dominate the eddy kinetic
92 energy field. This paper is structured as follows: the data sources and methodology are
93 described in section 2. Then, we present the climatology, energy ratios, and global sea-
94 sonality of the coherent eddy kinetic energy in subsection 3. Subsection 4 presents the
95 global climatology and seasonality of coherent eddy properties, followed by the seasonal
96 cycle and coherent eddy property time-series in regions dominated by coherent eddies
97 (subsection 6.1). We then focus our attention on the long-term changes of the coherent
98 eddy properties (section 5). Finally, section 7 summarizes the main results and discusses
99 the implications of this study.

100 2 Methods

101 2.1 Data

102 We use daily sea surface height (SSH) data are available by the Copernicus Ma-
103 rine Environment Monitoring Service in near real time (CMEMS, 2017). This gridded
104 product contains the sea surface height and geostrophic velocities with daily 0.25° res-
105 olution from January 1993 to 2019. The daily geostrophic velocities allowed us to com-
106 pute the KE and EKE over the satellite records. Mean and anomaly velocities are in in
107 reference to the full record mean of SSH (1993–2019), while all presented climatologies
108 correspond to the mean of the full record.

109 Over the same record, we use a mesoscale coherent eddy trajectory dataset released
110 by Chelton and Schlax (2013) to compare global statistics of coherent eddies in the present
111 study. This dataset was produced via an automated eddy identification developed by Chel-
112 ton et al. (2011).

113 The eddy identification procedure defines mesoscale eddies directly using the sea
114 surface height (SSH) field. This method was applied to avoid noise amplification in the
115 SSH field. Compared with the Okubo–Weiss parameter identification procedure, the SSH-
116 based procedure without the differentiation calculation of the SSH field effectively solves
117 the overestimation issue of eddy identification with less computational load. The dataset
118 retains only those eddies with lifetimes of four weeks or longer and provides trajectories
119 with 7-day time steps

120 Wind stress averaged over oceanic regions between 45S and 65S calculated from
121 the ERA interim reanalysis [Dee et al., 2011] (Figure 1b, black line) correlates well with
122 the annually averaged SAM (correlation 0.88). Wind stress increases from 1990 onward
123 at a rate consistent with the long-term trend (not shown) albeit masked by strong lev-
124 els of interannual variability. We also show how the ERA-interim wind stress has var-
125 ied within each ocean basin (Figure 1c). For this, we divide the Southern Ocean up into
126 the three sectors similar to those used by MH06 (Indian Ocean: 40E–150E, 57S–44S; Pa-
127 cific Ocean: 150E–288E, 62S–48S; and Atlantic Ocean: 325E–10E, 56S–46S). The regional
128 analysis indicates that the long-term trend in Southern Ocean wind stress is dominated
129 by changes in the Pacific sector.

130 2.2 Coherent eddy identification algorithm

131 TrackEddy is an autonomous eddy identification, tracking, and reconstruction al-
132 gorithm, which assumes eddies can be represented as isolated anisotropic Gaussian anom-
133 alies. The main and unique characteristic of the TrackEddy algorithm, which differs from
134 previous algorithms (Ashkezari et al., 2016; Chelton et al., 2007; Faghmous et al., 2015),
135 is its capability to reconstruct an optimal Gaussian anomaly for each identified eddy. This
136 Gaussian anomaly can be used to reconstruct the eddy velocities to calculate the TKE
137 associated with the identified coherent eddies. TrackEddy follows a similar work-flow to
138 previous methods using SSH. It starts with a single snapshot of SSHa, where potential
139 eddies are isolated using study-specific criteria. Generally, each study describes a strict

definition of what will be considered an eddy by constraining their size and/or shape. Then, the algorithm iterates at multiple discrete SSHa levels in which the coherent eddy definition is used to identify eddies. The identification algorithm at each discrete SSHa level is then applied to all time steps for which data are available. The following subsections present the TrackEddy algorithm structure, criteria, user-specified values, and energy calculation.

2.3 Kinetic Energy decomposition

Kinetic energy is commonly divided into the mean and time-varying components through a Reynolds decomposition. At a given time, the velocity field $\mathbf{u} = (u, v)$ is split into the time mean ($\bar{\mathbf{u}}$) and time varying components (\mathbf{u}'). Additionally, we further decompose the eddy kinetic energy into the eddy kinetic energy contained by coherent features (\mathbf{u}'_e) and non-coherent (\mathbf{u}'_n). Therefore the KE equation can be written as:

$$\text{KE} = \underbrace{\bar{u}^2 + \bar{v}^2}_{\text{MKE}} + \underbrace{u'_e^2 + v'_e^2}_{\text{CEKE}} + \underbrace{u'_n^2 + v'_n^2}_{\text{nCEKE}} + \mathcal{O}_c^2 + \mathcal{O}^2 \quad (1)$$

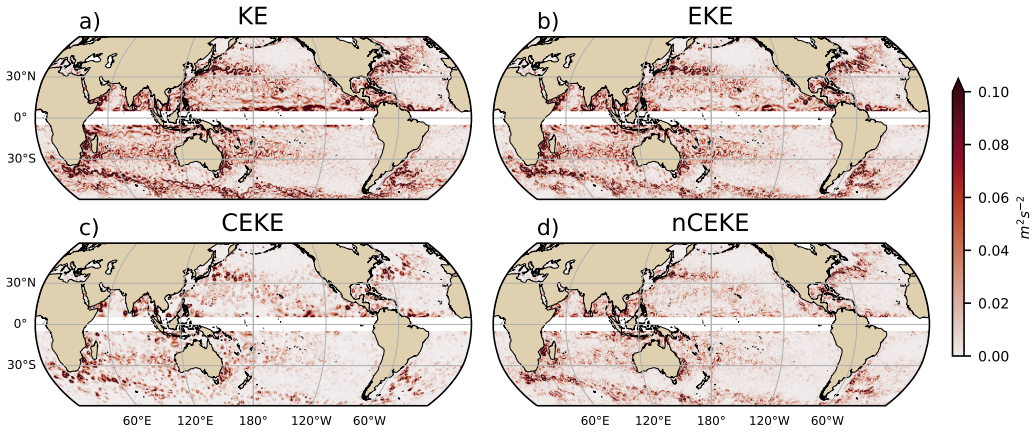
Due to the properties of this decomposition, the second order term \mathcal{O}^2 is zero when averaged over the same period as $\bar{\mathbf{u}}$. However, \mathcal{O}_c^2 is only negligible when averaged in time and space. For more information about the decomposition of the field into coherent features and non-coherent features refer to Martínez-Moreno et al. (2019). A global snapshot of each component of kinetic energy decomposition is shown in figure 1, where the imprint of the coherent eddies corresponds to rings of kinetic energy.

3 Global Coherent Eddy Energetics

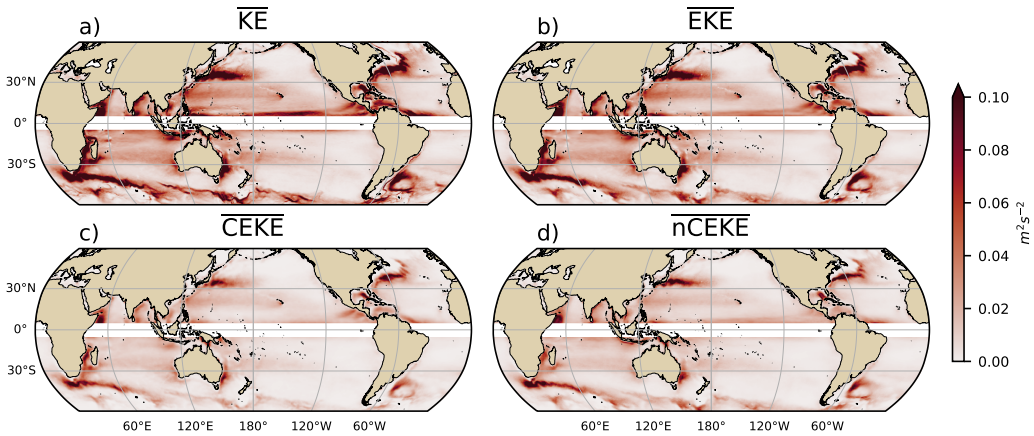
Figure 2

- All KE components have large energy contents in the boundary currents and antarctic circumpolar current.
- In many cases is the same, but there actually some differences There are several regions where the coherent component is larger than the non-coherent, we will investigate these in more detail in section XX.

Figure 3



158 **Figure 1.** Snapshot of surface kinetic energy (\overline{KE}), surface eddy kinetic energy (\overline{EKE}),
 159 surface coherent eddy kinetic energy (\overline{CEKE}), and surface non-coherent eddy kinetic energy
 160 (\overline{nCEKE}) for the 1st of January 2017.



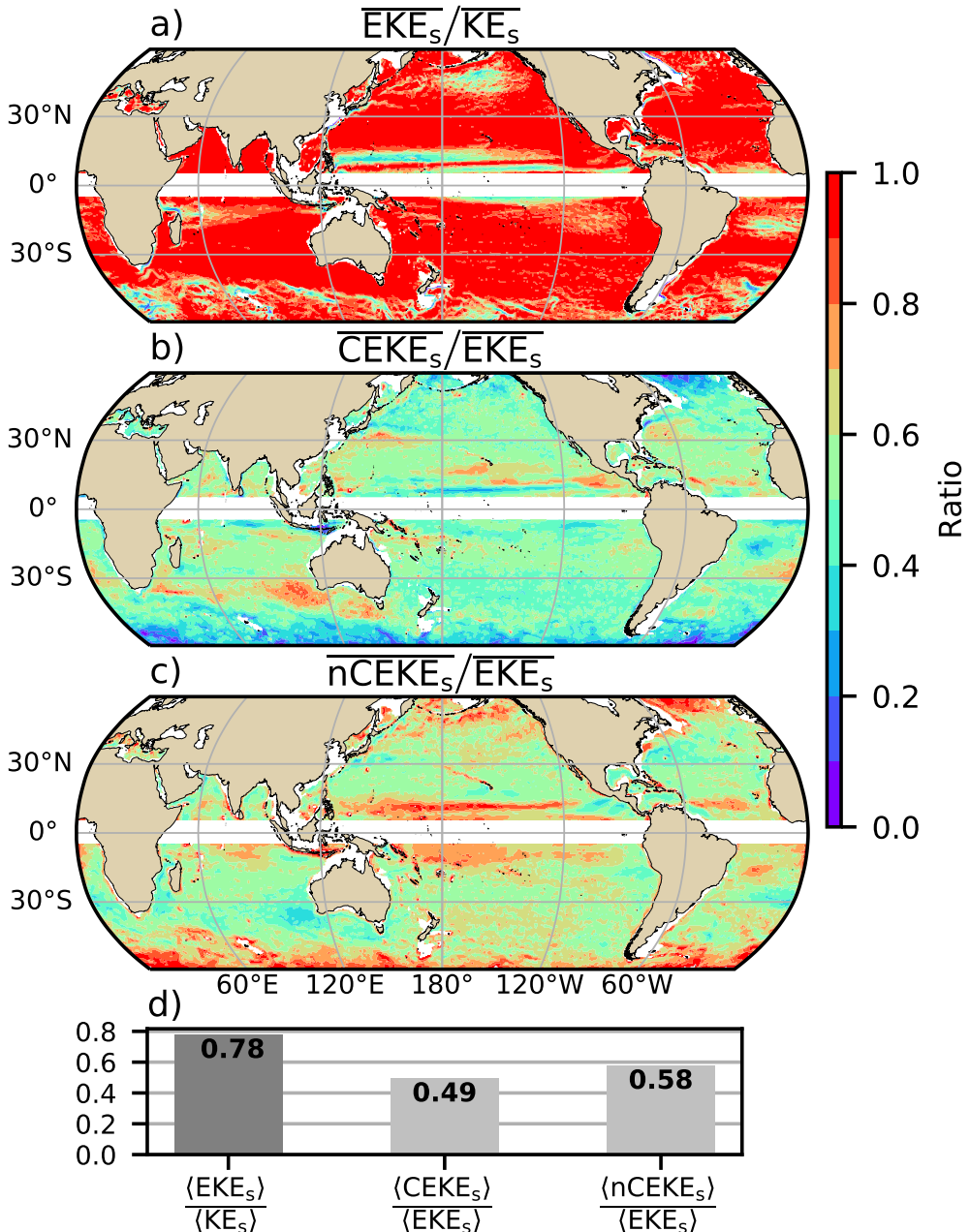
168 **Figure 2.** Climatology of surface kinetic energy (\overline{KE}), surface eddy kinetic energy (\overline{EKE}),
 169 surface coherent eddy kinetic energy (\overline{CEKE}), and surface non-coherent eddy kinetic energy
 170 (\overline{nCEKE}) between 1993-2018.

- $\overline{\text{EKE}}$ is responsible of almost all the $\overline{\text{KE}}$ across the ocean, except for regions with persistent currents over time, such as the mean boundary current locations, equatorial pacific currents and regions in the Antarctic Circumpolar current, where the EKE explains around 40% of the $\overline{\text{KE}}$
- This estimate is consistent with that of Chelton.
- EKE Explains 80% of $\overline{\text{KE}}$, while $\overline{\text{CEKE}}$ is 45% of $\overline{\text{EKE}}$ and $\overline{\text{nCEKE}}$ is 60% of $\overline{\text{EKE}}$
- $\overline{\text{CEKE}}$ is large equatorwards from the Kuroshio current and Agulhas current.
- Areas with the largest coherent contribution are located in the South of Australia $\overline{\text{CEKE}}$ and South Atlantic
-
- $\overline{\text{nCEKE}}$ has a large amount of energy at high latitudes, this could be a consequence of the satellites not resolving the mesoscale coherent eddies.
- Global averages of the ratios show $\overline{\text{EKE}}$ explains around 78% of the ocean *MKE* field, while coherent eddies and non coherent eddy features contain 49% and 59% per decade. Note this values don't add to 1 as there are cross terms that contain around XX% of the total energy.

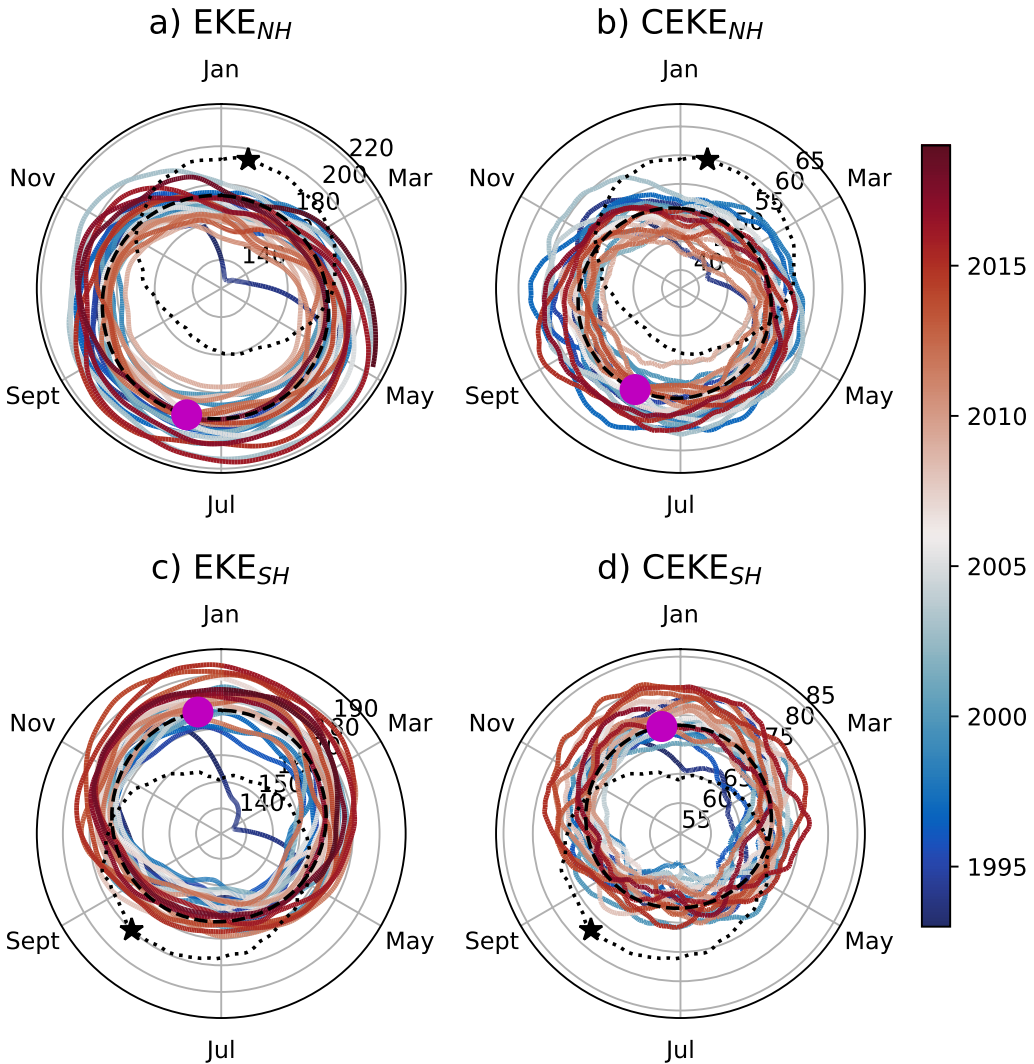
3.0.1 Seasonality

Figure 4

- The hemisphere seasonality show the EKE and CEKE peak in summer.
- Response of the EKE and CEKE show a seasonal lag of \sim 6 months to the forcing of the Winds. Make sure to note the maximum over the hemisphere, locally, the winds may peak in different months.
- Methods, explain more about winds or here.
- The coherent eddy field show a large interannual variability.
- In the Southern Ocean we observe a concentric growth as time passes, which support the increasing trends in the Southern Ocean observed by (Hogg et al., 2015; Martínez-Moreno et al., 2019, 2021)
- Point that in the northern hemisphere in winter the CEKE appears to be decreasing.



189 **Figure 3.** Ratios of the kinetic energy components. a) Map of the proportion of mean eddy
 190 kinetic energy (EKE_s) versus mean kinetic energy (\overline{KE}_s); b) Map of the percentage of mean co-
 191 herent eddy kinetic energy (\overline{CEKE}_s) versus mean eddy kinetic energy (\overline{EKE}_s); c) Map of the
 192 percentage of mean non-coherent eddy kinetic energy (\overline{nCEKE}_s) versus mean eddy kinetic energy
 193 (\overline{EKE}_s); d) Global averaged percentage of mean eddy kinetic energy ($\langle \overline{EKE} \rangle$) versus the global
 194 mean kinetic energy ($\langle \overline{KE} \rangle$), and percentage of mean coherent eddy kinetic energy ($\langle \overline{CEKE} \rangle$)
 195 and mean non coherent eddy kinetic energy ($\langle \overline{nCEKE} \rangle$) versus global mean eddy kinetic energy
 196 ($\langle \overline{EKE} \rangle$).



210 **Figure 4.** Hemispherical seasonality of eddy kinetic energy (EKE), coherent eddy kinetic en-
 211 ergy (CEKE). Panels a, and b show the northern hemisphere seasonal cycle, while panels c, and
 212 d correspond to the southern hemisphere. Dashed lines correspond to the seasonal cycle of the
 213 fields and dotted lines show the seasonal cycle of the wind magnitude smoothed over 120 days
 214 (moving average). The green and magenta stars show the maximum of the seasonal cycle for the
 215 kinetic energy components and the wind magnitude, respectively. The line colors show the year.

216 **4 Global Coherent Eddy Statistics**

217 **Figure 5**

- 218 • A comparison with previous identified numbers show a consistent pattern in the
219 eddy count. The difference in the magnitude could be a consequence of Chelton
220 et al. (2007) filtering the coherent eddies with lifespans longer than 16 weeks.
- 221 • Both datasets show a large number of eddies in the East North Pacific, East North
222 Atlantic, as well as the East South Pacific, East South Atlantic and East Indian
223 Ocean.
- 224 • While the number of eddies detected in the tropics is quite small.
- 225 • Furthermore, there are hotspots of numbers of eddies in other regions of the ocean,
226 such as boundary currents and the Antarctic Circumpolar Current.
- 227 • An interesting feature shown in both datasets is a predominant patchiness where
228 the count of the eddies is much larger. These puzzling pattern remains unknown.
229 Although it looks like a propagation pattern, it could be that eddies persist for
230 longer in those areas.
- 231 • The eddy amplitude as expected is maximum at the boundary currents and hotspots
232 in the southern ocean.
- 233 • Interior of the gyres we can observe that there is an important amplitude of the
234 coherent eddy field.
- 235 • Preferred eddy amplitude sign in boundary currents; positive amplitude polewards
236 to the boundary current mean location, and negative amplitude equatorwards. This
237 is consistent with the shed of coherent eddies from the boundary currents.
- 238 • There regions with large CEKE ratio show also a large coherent eddy amplitude.
- 239 • Absolute eddy amplitude has the similar signature as CEKE.

245 **4.0.1 Seasonality**

246 **Figure 6**

- 247 • Seasonality of the number of eddies in the Northern Hemisphere peaks on May,
248 while the Southern Hemisphere peaks on October.
- 249 • The seasonality of the amplitude of the eddies is consistent with those of the Co-
250 herent eddy kinetic energy.

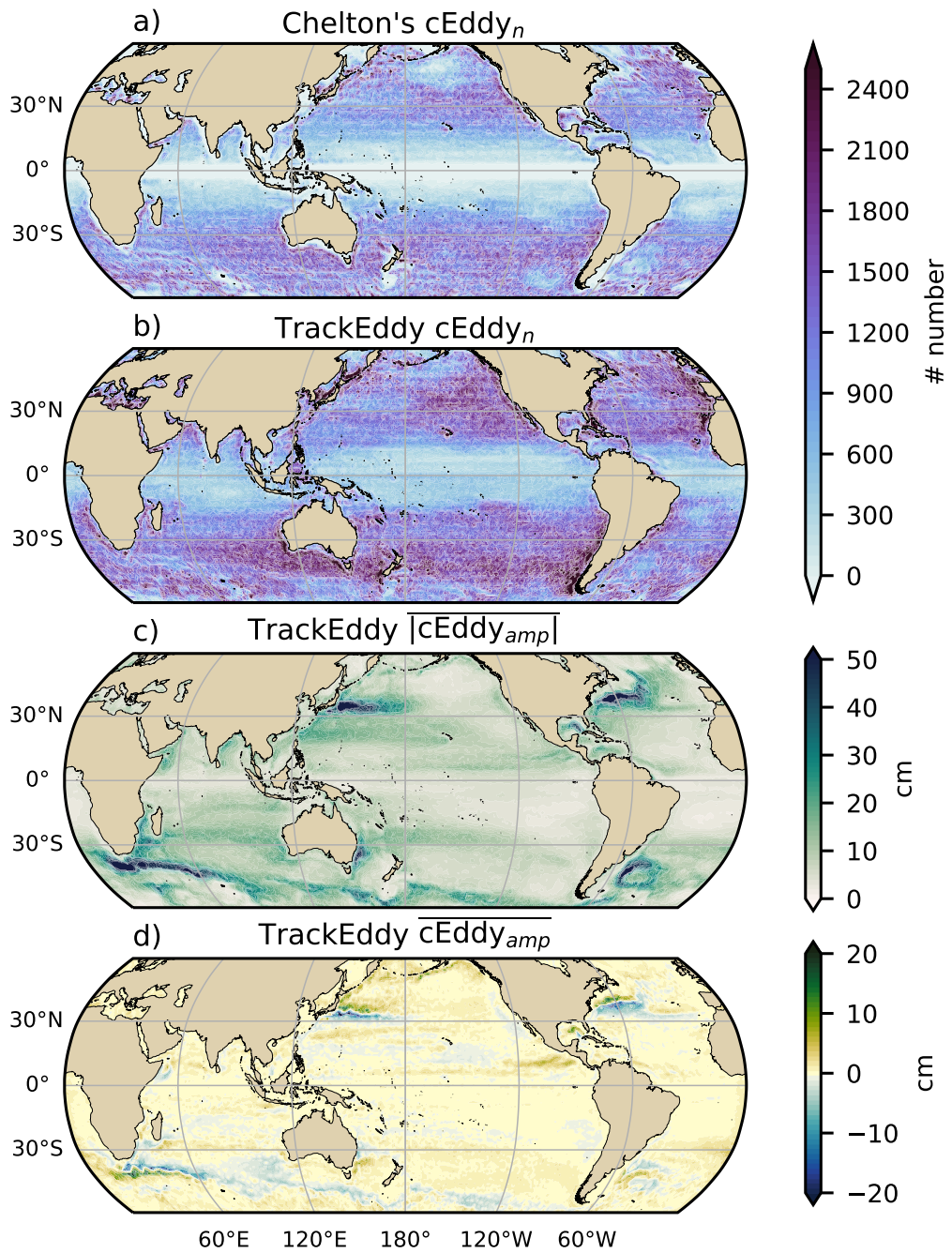


Figure 5. Climatology of the coherent eddy statistics. a) Climatology of the number of coherent eddies ($cEddy_n$) identified by Chelton et al. (2007); b) Climatology of the number of coherent eddies ($cEddy_n$) identified by Martínez-Moreno et al. (2019); c) Climatology of the mean absolute coherent eddy amplitude ($cEddy_{amp}$). d) Climatology of the mean coherent eddy amplitude ($cEddy_{amp}$).

- Interestingly, there is a 3 month lag to between the winds and the seasonality of the number of eddies, while the eddy amplitude responds approximately 6 months after the maximum winds.
- Note that both coherent eddy amplitudes seem to peak around the same time.
- If we look closely, the growing-shrinking concentric circles correspond to an increasing-decreasing trend. These are particularly obvious as a decrease in the eddy number in the Southern Hemisphere, and a increase in the eddy amplitude.

Figure 6

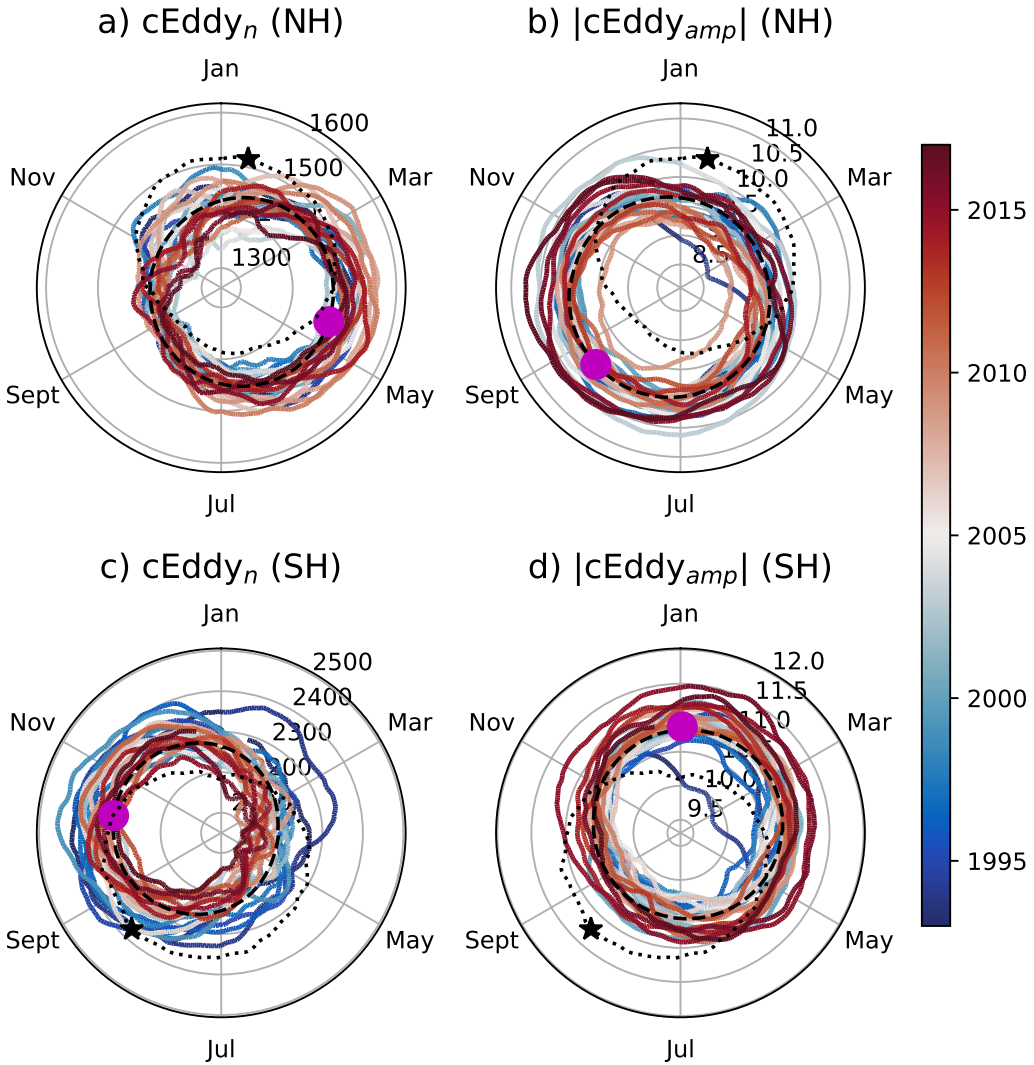
- a

5 Trends**Figure 13**

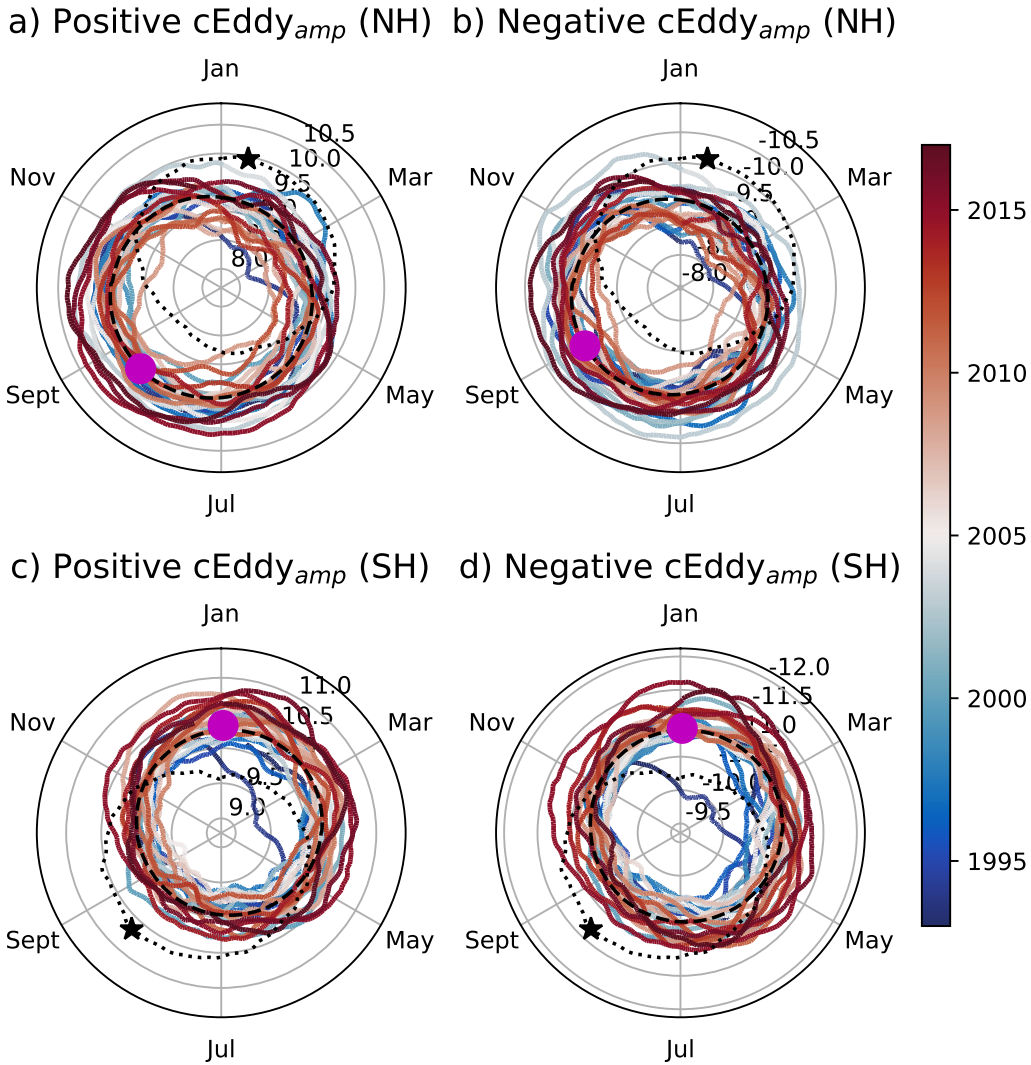
- The number and amplitude of coherent eddies from two eddy tracking algorithms show consistent trend patterns.
- In particular, we observe a decrease in the number of eddies in the southern ocean, as well as sectors in the North Atlantic and North Pacific.
- Meanwhile the amplitude seems to be increasing in those same regions.
- Some of these regions have undergone a readjustment to stronger winds, thus the observed trends in the eddy amplitude suggests an intensification of the coherent eddy field to an increase in the forcing.
- This increase is consistent with Martínez-Moreno et al. (2021)

6 Regional**6.1 Boundary Currents****Figure 10**

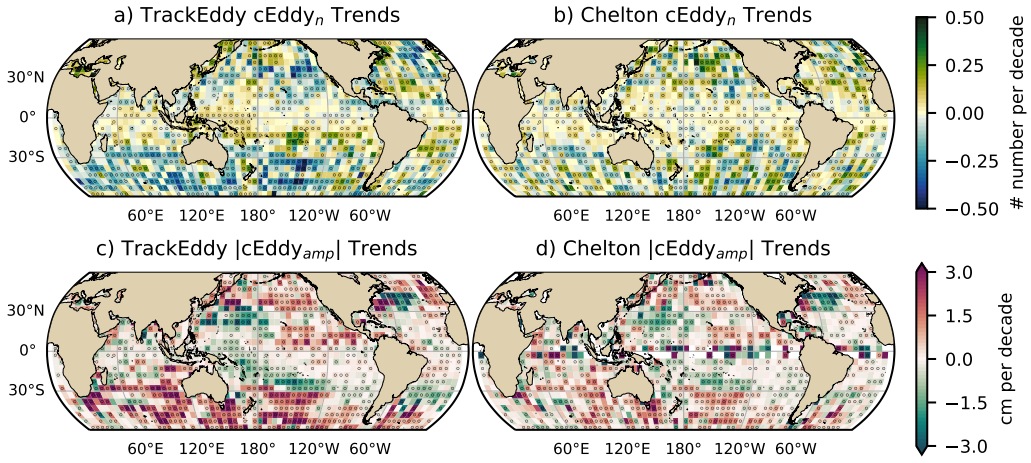
- Described similar to figure 7, 8, and 9
- Note that boundary currents have a consistent seasonal cycle in the positive and negative eddy amplitude.
- As expected, the seasonal cycle is opposite to BC in the northern hemisphere.



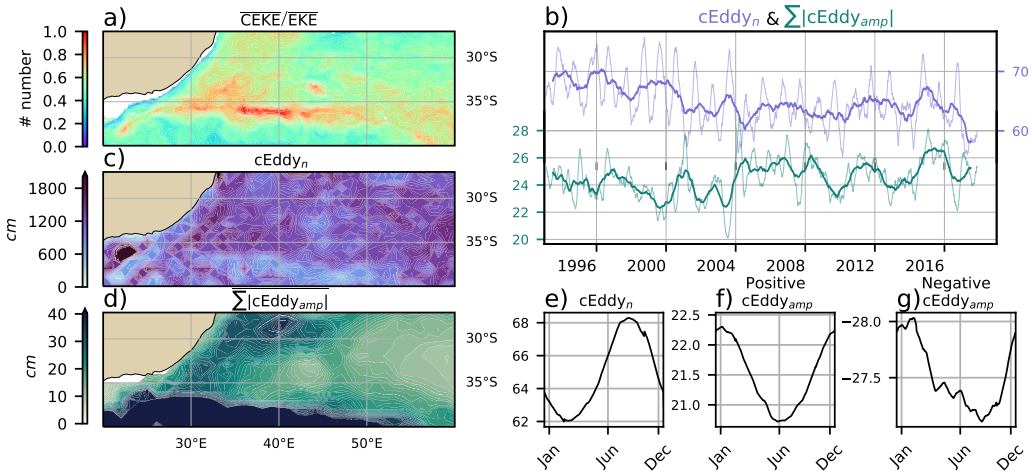
258 **Figure 6.** Hemispherical seasonality of the coherent eddy statistics; a,e) seasonal cycle of the
 259 number of coherent eddies ($cEddy_n$); b,f) seasonal cycle of the mean coherent eddy amplitude
 260 ($cEddy_{amp}$); c,g) seasonal cycle of the warm core coherent eddies amplitude (positive $cEddy_{amp}$);
 261 d,h) seasonal cycle of the cold core coherent eddies amplitude (negative $cEddy_{amp}$). Panels a,b
 262 and c show the northern hemisphere seasonal cycle, while panels d,e, and f correspond to the
 263 southern hemisphere. Dashed lines correspond to the seasonal cycle of the fields and dotted lines
 264 show the seasonal cycle of the wind magnitude smoothed over 120 days (moving average). The
 265 green and magenta stars show the maximum of the seasonal cycle for each field and the wind
 266 magnitude, respectively. The line colors show the year.



269 **Figure 7.** Hemispherical seasonality of the coherent eddy statistics; a,e) seasonal cycle of the
 270 number of coherent eddies ($cEddy_n$); b,f) seasonal cycle of the mean coherent eddy amplitude
 271 ($cEddy_{amp}$); c,g) seasonal cycle of the warm core coherent eddies amplitude (positive $cEddy_{amp}$);
 272 d,h) seasonal cycle of the cold core coherent eddies amplitude (negative $cEddy_{amp}$). Panels a,b
 273 and c show the northern hemisphere seasonal cycle, while panels d,e, and f correspond to the
 274 southern hemisphere. Dashed lines correspond to the seasonal cycle of the fields and dotted lines
 275 show the seasonal cycle of the wind magnitude smoothed over 120 days (moving average). The
 276 green and magenta stars show the maximum of the seasonal cycle for each field and the wind
 277 magnitude, respectively. The line colors show the year.



289 **Figure 8.** Trends of coherent eddy statistics. a) and b) Trends of the number of identified
 290 coherent eddies from satellite observations identified using TrackEddy, and those reported in
 291 Chelton's dataset. c) and e) Trends of the mean absolute value of identified coherent eddies am-
 292 plitude from satellite observations identified using TrackEddy, and those reported in Chelton's
 293 dataset. Gray stippling shows regions that are statistically significant above the 95% confidence
 294 level.



302 **Figure 9.** Same as Figure 12 but for the Agulhas Current.

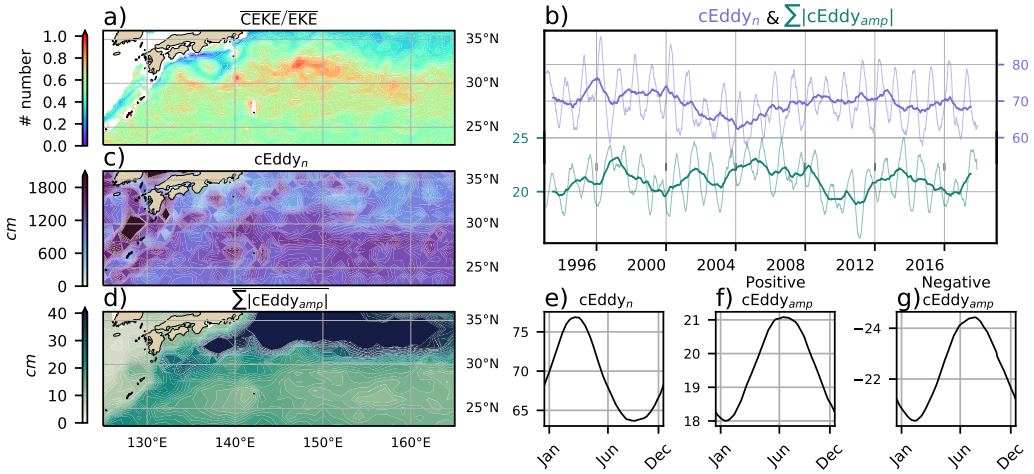


Figure 10. Same as Figure 12 but for the Kuroshio Current.

307

303

Figure 11

304

305

306

- Described similar to figure 7, 8, and 9
- Note that boundary currents have a consistent seasonal cycle in the positive and negative eddy amplitude.

308

Figure 12

309

310

311

312

- Described similar to figure 7, 8, and 9
- Note that boundary currents have a consistent seasonal cycle in the positive and negative eddy amplitude.
- Delete Fig 11 or 12, they are really similar. What do you think?

314

6.2 Eastern currents

315

Figure 7

316

317

318

319

320

- South of the Leeuwin Current there is an important dominance fo the coherent eddy field, where it explains around 80% of the eddy kinetic energy.
- Although this region does not have a large EKE, we can observe a considerable amount of eddies across the region, but more importantly the coherent eddy amplitude is particularly large in those regions with coherent eddy dominance.

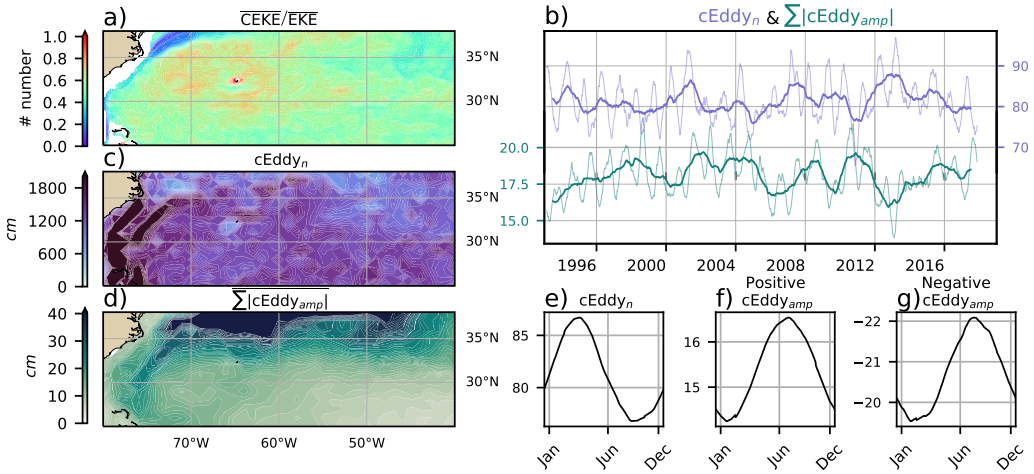
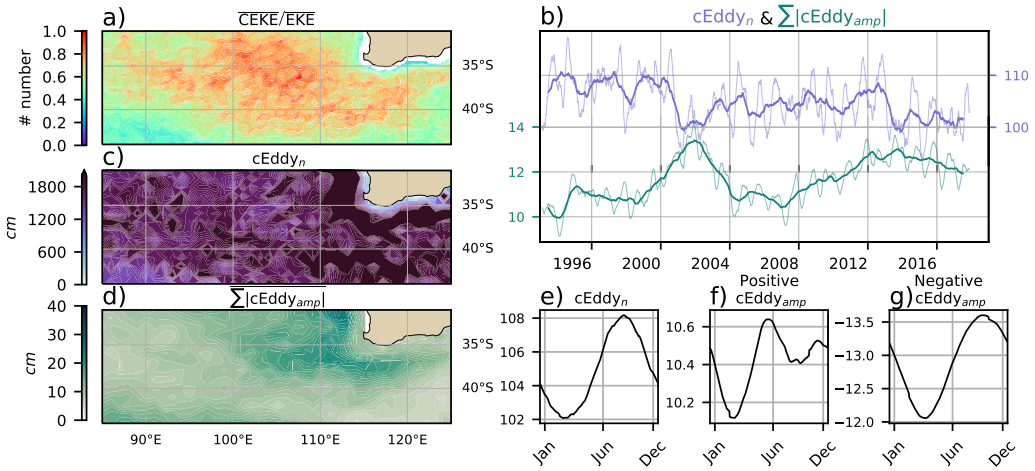


Figure 11. Move to supplementary Same as Figure 12 but for the Gulf Stream.

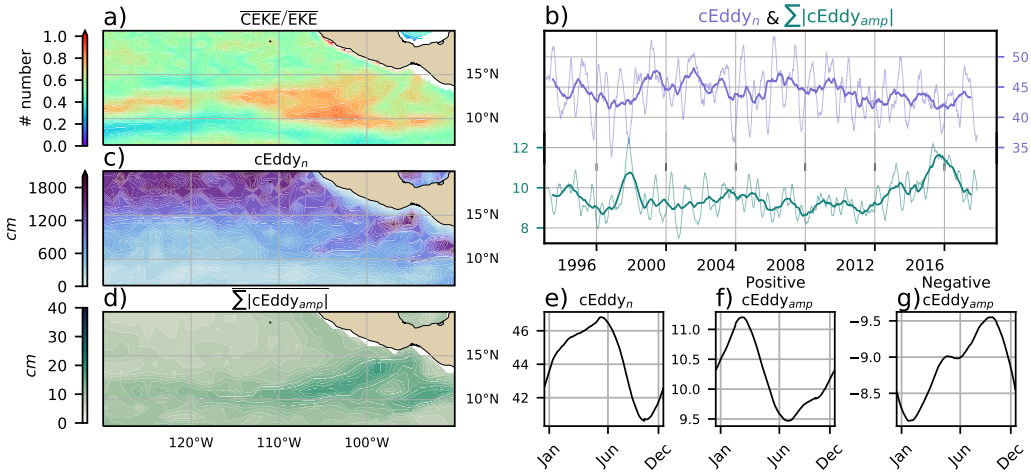
- The solid lines show an decrease in the number of eddies, but an increase in the eddy amplitude.
- Moreover, the coherent eddy number peaks in August.
- Meanwhile coherent eddies with the positive amplitude have a smaller amplitude than the negative, furthermore, the positive eddies peak in Jun and show a inter-annual modulation, while the negative eddies peak in October.
- Research regional dynamics (Add here why we may expect this response.)

Figure 9

- Here we observe that the number of eddies and eddy amplitude are large in the area where the coherent eddies dominate the eddy field.
- Dynamically, in this region eddies are generated due to Rossby wave propagation along the coast that becomes unstable and sheds eddies at the Tehuantepec Gulf.
- The seasonal cycle shows a peak in Jun, while the positive amplitude is observed in March and the negative amplitude maximum occurs in September.
- Research regional dynamics (Add here why we may expect this response.)



328 **Figure 12.** Climatology of the eddy field and coherent eddy field at the Leeuwin Current. a)
 329 Ratio of mean coherent eddy kinetic energy ($\overline{\text{CEKE}}$) versus mean eddy kinetic energy ($\overline{\text{EKE}}$); b)
 330 Thick lines show the running average over 2 years and thin lines show the running average over
 331 90 days of the coherent eddy number sum and the average absolute coherent eddy amplitude; c)
 332 Map of the number of eddies; d) Map of the average absolute coherent eddy amplitude; e) Sea-
 333 sonal cycle of the number of eddies f) Seasonal cycle of the positive coherent eddy amplitude. g)
 334 Seasonal cycle of the negative coherent eddy amplitude.



343 **Figure 13.** Same as Figure 12 but for the East Tropical Pacific.

344 **7 Summary and Conclusions**

345 **Acknowledgments**

346 **References**

- 347 Arbic, B. K., Polzin, K. L., Scott, R. B., Richman, J. G., & Shriver, J. F. (2013).
 On Eddy Viscosity, Energy Cascades, and the Horizontal Resolution of Gridded
 Satellite Altimeter Products*. *Journal of Physical Oceanography*, 43(2), 283–300.
 doi: 10.1175/jpo-d-11-0240.1
- 351 Ashkezari, M. D., Hill, C. N., Follett, C. N., Forget, G., & Follows, M. J. (2016).
 Oceanic eddy detection and lifetime forecast using machine learning methods.
Geophysical Research Letters, 43(23). doi: 10.1002/2016gl071269
- 354 Beron-Vera, F. J., Wang, Y., Olascoaga, M. J., Goni, G. J., & Haller, G. (2013). Ob-
 jective Detection of Oceanic Eddies and the Agulhas Leakage. *Journal of Physical
 Oceanography*, 43(7), 1426–1438. doi: 10.1175/JPO-D-12-0171.1
- 357 Bouali, M., Sato, O. T., & Polito, P. S. (2017). Temporal trends in sea surface tem-
 perature gradients in the South Atlantic Ocean. *Remote Sensing of Environment*,
 194, 100–114. doi: 10.1016/j.rse.2017.03.008
- 360 Callies, J., Flierl, G., Ferrari, R., & Fox-Kemper, B. (2015). The role of mixed-layer
 instabilities in submesoscale turbulence. *Journal of Fluid Mechanics*, 788, 5–41.
 doi: 10.1017/jfm.2015.700
- 363 Cane, M. A., Clement, A. C., Kaplan, A., Kushnir, Y., Pozdnyakov, D., Seager, R.,
 ... Murtugudde, R. (1997). Twentieth-Century Sea Surface Temperature Trends.
Science, 275(5302), 957–960. doi: 10.1126/science.275.5302.957
- 366 Chelton, D. B., Gaube, P., Schlax, M. G., Early, J. J., & Samelson, R. M. (2011).
 The influence of nonlinear mesoscale eddies on near-surface oceanic chlorophyll.
Science, 334(6054), 328-32. doi: 10.1126/science.1208897
- 369 Chelton, D. B., Schlax, M. G., Samelson, R. M., & de Szoeke, R. A. (2007). Global
 observations of large oceanic eddies. *Geophysical Research Letters*, 34(15),
 L15606. doi: 10.1029/2007GL030812
- 372 CMEMS. (2017). The Ssalto/Duacs altimeter products were produced and dis-
 tributed by the Copernicus Marine and Environment Monitoring Service. *Aviso
 Dataset*. Retrieved from <https://www.aviso.altimetry.fr/>

- 375 Cui, W., Wang, W., Zhang, J., & Yang, J. (2020). Identification and census statistics
376 of multicore eddies based on sea surface height data in global oceans. *Acta*
377 *Oceanologica Sinica*, 39(1), 41–51. doi: 10.1007/s13131-019-1519-y
- 378 Faghmous, J. H., Frenger, I., Yao, Y., Warmka, R., Lindell, A., & Kumar, V. (2015,
379 6). A daily global mesoscale ocean eddy dataset from satellite altimetry. *Scientific*
380 *Data*, 2, 150028 EP -. doi: 10.1038/sdata.2015.28
- 381 Ferrari, R., & Wunsch, C. (2009). Ocean Circulation Kinetic Energy: Reservoirs,
382 Sources, and Sinks. *Annual Review of Fluid Mechanics*, 41(1), 253–282. doi: 10
383 .1146/annurev.fluid.40.111406.102139
- 384 Frenger, I., Gruber, N., Knutti, R., & Münnich, M. (2013). Imprint of Southern
385 Ocean eddies on winds, clouds and rainfall. *Nature Geoscience*, 6(8), 608 EP -.
386 doi: 10.1038/ngeo1863
- 387 Frenger, I., Münnich, M., Gruber, N., & Knutti, R. (2015). Southern Ocean eddy
388 phenomenology. *Journal of Geophysical Research: Oceans*, 120(11), 7413-7449.
389 doi: 10.1002/2015JC011047
- 390 Fu, L., Chelton, D., Le Traon, P., & Oceanography, M. R. (2010). Eddy dynamics
391 from satellite altimetry. *Oceanography*, 23(4), 14-25. doi: 10.2307/24860859
- 392 Gill, A., Green, J., & Simmons, A. (1974). Energy partition in the large-scale ocean
393 circulation and the production of mid-ocean eddies. *Deep Sea Res Oceanogr Abstr*,
394 21(7), 499-528. doi: 10.1016/0011-7471(74)90010-2
- 395 Hogg, A. M., & Blundell, J. R. (2006). Interdecadal variability of the southern
396 ocean. *Journal of Physical Oceanography*, 36(8), 1626-1645. doi: 10.1175/
397 JPO2934.1
- 398 Hogg, A. M., Meredith, M. P., Chambers, D. P., Abrahamsen, E. P., Hughes,
399 C. W., & Morrison, A. K. (2015). Recent trends in the Southern Ocean
400 eddy field. *Journal of Geophysical Research: Oceans*, 120(1), 257-267. doi:
401 10.1002/2014JC010470
- 402 Hu, S., Sprintall, J., Guan, C., McPhaden, M. J., Wang, F., Hu, D., & Cai,
403 W. (2020, 2). Deep-reaching acceleration of global mean ocean circula-
404 tion over the past two decades. *Science Advances*, 6(6), eaax7727. doi:
405 10.1126/sciadv.aax7727
- 406 Kang, D., & Curchitser, E. N. (2017). On the Evaluation of Seasonal Variability of
407 the Ocean Kinetic Energy. *Geophysical Research Letters*, 47, 1675-1583. doi: 10

- 408 .1175/JPO-D-17-0063.1
- 409 Li, G., Cheng, L., Zhu, J., Trenberth, K. E., Mann, M. E., & Abraham, J. P. (2020).
410 Increasing ocean stratification over the past half-century. *Nature Climate Change*,
411 1–8. doi: 10.1038/s41558-020-00918-2
- 412 Martínez-Moreno, J., Hogg, A. M., England, M., Constantinou, N. C., Kiss, A. E.,
413 & Morrison, A. K. (2021). Global changes in oceanic mesoscale currents over the
414 satellite altimetry record. *Journal of Advances in Modeling Earth Systems*, 0(ja).
415 doi: 10.1029/2019MS001769
- 416 Martínez-Moreno, J., Hogg, A. M., Kiss, A. E., Constantinou, N. C., & Mor-
417 rison, A. K. (2019). Kinetic energy of eddy-like features from sea surface
418 altimetry. *Journal of Advances in Modeling Earth Systems*, 0(ja). doi:
419 10.1029/2019MS001769
- 420 Patel, R. S., Llort, J., Strutton, P. G., Phillips, H. E., Moreau, S., Pardo, P. C.,
421 & Lenton, A. (2020). The Biogeochemical Structure of Southern Ocean
422 Mesoscale Eddies. *Journal of Geophysical Research: Oceans*, 125(8). doi:
423 10.1029/2020jc016115
- 424 Pilo, G. S., Mata, M. M., & Azevedo, J. L. L. (2015). Eddy surface properties and
425 propagation at Southern Hemisphere western boundary current systems. *Ocean
426 Science*, 11(4), 629–641. doi: 10.5194/os-11-629-2015
- 427 Qiu, B. (1999). Seasonal Eddy Field Modulation of the North Pacific Subtropical
428 Countercurrent: TOPEX/Poseidon Observations and Theory. *Journal of Physical
429 Oceanography*, 29(10), 2471–2486. doi: 10.1175/1520-0485(1999)029<2471:sefmot>2
430 .0.co;2
- 431 Qiu, B., & Chen, S. (2004). Seasonal Modulations in the Eddy Field of the South
432 Pacific Ocean. *Journal of Physical Oceanography*, 34(7), 1515–1527. doi: 10.1175/
433 1520-0485(2004)034<1515:smitef>2.0.co;2
- 434 Qiu, B., Chen, S., Klein, P., Sasaki, H., & Sasai, Y. (2014). Seasonal Mesoscale
435 and Submesoscale Eddy Variability along the North Pacific Subtropical Coun-
436 tercurrent. *Journal of Physical Oceanography*, 44(12), 3079–3098. doi:
437 10.1175/jpo-d-14-0071.1
- 438 Ruela, R., Sousa, M. C., deCastro, M., & Dias, J. M. (2020). Global and regional
439 evolution of sea surface temperature under climate change. *Global and Planetary
440 Change*, 190, 103190. doi: 10.1016/j.gloplacha.2020.103190

- 441 Sasaki, H., Klein, P., Qiu, B., & Sasai, Y. (2014). Impact of oceanic-scale inter-
442 actions on the seasonal modulation of ocean dynamics by the atmosphere. *Nature
443 Communications*, 5(1), 5636. doi: 10.1038/ncomms6636
- 444 Schubert, R., Schwarzkopf, F. U., Baschek, B., & Biastoch, A. (2019). Submesoscale
445 Impacts on Mesoscale Agulhas Dynamics. *Journal of Advances in Modeling Earth
446 Systems*, 11(8), 2745–2767. doi: 10.1029/2019ms001724
- 447 Siegel, D., Peterson, P., DJ, M., Maritorena, S., & Nelson, N. (2011). Bio-optical
448 footprints created by mesoscale eddies in the Sargasso Sea. *Geophysical Research
449 Letters*, 38(13), n/a-n/a. doi: 10.1029/2011GL047660
- 450 Uchida, T., Abernathey, R., & Smith, S. (2017). Seasonality of eddy kinetic energy
451 in an eddy permitting global climate model. *Ocean Modelling*, 118, 41-58. doi: 10
452 .1016/j.ocemod.2017.08.006
- 453 Wunsch, C. (2020). Is The Ocean Speeding Up? Ocean Surface Energy Trends.
454 *Journal of Physical Oceanography*, 50(11), 1–45. doi: 10.1175/jpo-d-20-0082.1
- 455 Wunsch, C., & Ferrari, R. (2004). VERTICAL MIXING, ENERGY, AND THE
456 GENERAL CIRCULATION OF THE OCEANS. *Annual Review of Fluid Me-
457 chanics*, 36(1), 281–314. doi: 10.1146/annurev.fluid.36.050802.122121
- 458 Wyrtki, K., Magaard, L., & Hager, J. (1976). Eddy energy in the oceans. *Journal of
459 Geophysical Research*, 81(15), 2641-2646. doi: 10.1029/JC081i015p02641